



HAL
open science

Competition within low-density bacterial populations as an unexpected factor regulating carbon decomposition in bulk soil

Alexandre Coche, Tristan Babey, Alain Rapaport, Laure Vieublé Gonod, Patricia Garnier, Naoise Nunan, Jean-Raynald de Dreuzy

► To cite this version:

Alexandre Coche, Tristan Babey, Alain Rapaport, Laure Vieublé Gonod, Patricia Garnier, et al.. Competition within low-density bacterial populations as an unexpected factor regulating carbon decomposition in bulk soil. *Soil Biology and Biochemistry*, 2022, 164 (108423), <10.1016/j.soilbio.2021.108423>. <insu-03347522v3>

HAL Id: insu-03347522

<https://insu.hal.science/insu-03347522v3>

Submitted on 23 Nov 2021

HAL is a multi-disciplinary open access archive for the deposit and dissemination of scientific research documents, whether they are published or not. The documents may come from teaching and research institutions in France or abroad, or from public or private research centers.

L'archive ouverte pluridisciplinaire HAL, est destinée au dépôt et à la diffusion de documents scientifiques de niveau recherche, publiés ou non, émanant des établissements d'enseignement et de recherche français ou étrangers, des laboratoires publics ou privés.



HAL Authorization

1 **Competition within low-density bacterial populations as an**
2 **unexpected factor regulating carbon decomposition in bulk soil**

3 Alexandre Coche^{a*}, Tristan Babey^b, Alain Rapaport^c, Laure Vieublé Gonod^d,
4 Patricia Garnier^d, Naoise Nunan^{e,f}, Jean-Raynald de Dreuzy^a

5 ^a Univ Rennes, CNRS, Géosciences Rennes - UMR 6118, F-35000 Rennes, France

6 ^b Stanford University, Department of Earth System Science, Stanford, USA

7 ^c MISTEA, Univ. Montpellier, INRAE, Montpellier SupAgro, France

8 ^d UMR Ecosys, INRAE, AgroParisTech, Université Paris-Saclay, 78850, Thiverval Grignon,
9 France

10 ^e Sorbonne Université, CNRS, IRD, INRAE, P7, UPEC, Institute of Ecology and Environmental
11 Sciences—Paris, 4 place Jussieu, 75005 Paris, France

12 ^f Department of Soil & Environment, Swedish University of Agricultural Sciences, P.O. Box
13 7014, 75007 Uppsala, Sweden

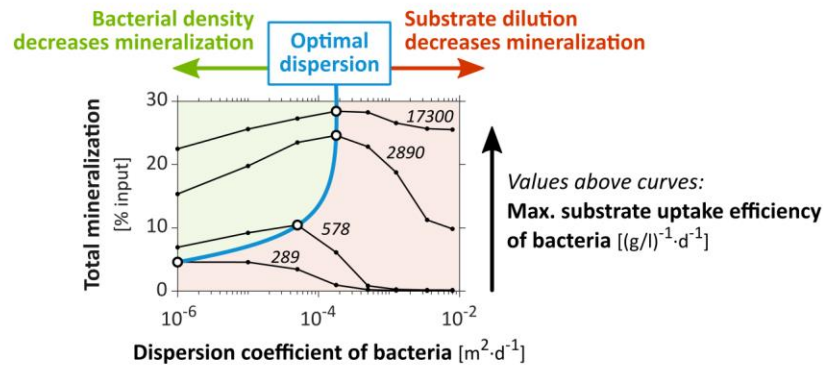
14 * Corresponding author. *E-mail address*: alexandre.coche@univ-rennes1.fr (A. Coche)

15 **Abstract**

16 Bacterial decomposition of organic matter in soils is generally believed to be mainly
17 controlled by the access bacteria have to organic substrate. The influence of bacterial traits
18 on this control has, however, received little attention. Using the substrate-dependent
19 Monod growth model, we develop a bioreactive transport model to screen the interactive
20 impacts of spatial dispersion and bacterial traits on mineralization. Bacterial traits primarily

21 involved in the bacterial response to the substrate concentration, such as the maximum
22 specific uptake rate and efficiency, the adaptation time of the uptake rate and the initial
23 population density, are considered. We compare the model results with two sets of
24 previously performed cm-scale soil-core experiments in which the mineralization of the
25 pesticide 2,4-D was measured under well-controlled initial distributions and transport
26 conditions. Bacterial dispersion away from the initial substrate location induced a significant
27 increase in 2,4-D mineralization. It reveals an increase of specific uptake rates at lower
28 bacterial densities, more than compensating the decrease of specific uptake rates caused by
29 substrate dilution. This regulation of bacterial activities by density, caused by the local
30 depletion of substrate by competing bacteria, becomes dominant for bacteria with an
31 efficient uptake of substrate at low substrate concentrations (a common feature of
32 oligotrophs). Such oligotrophs, commonly found in soils, compete with each other for
33 substrate even at remarkably low population densities. The ratio-dependent Contois growth
34 model, which includes a density regulation in the expression of the uptake efficiency, is more
35 accurate and convenient to calibrate than the substrate-dependent Monod model, at least
36 under these conditions. In view of their strong interactions, bioreactive and transport
37 processes cannot be handled independently but should be integrated, in particular when
38 reactive processes of interest are carried out by oligotrophs.

39 *Keywords:* biodegradation of organic matter; heterogeneous spatial distributions;
40 bioreactive transport model; competition for substrate; bacterial traits; ratio-dependent
41 growth



42

43 Highlights

- 44 - The impact of spatial distributions on decomposition depends on bacterial traits
- 45 - Decomposition can be reduced by competition between bacteria even at low densities
- 46 - Bacterial density regulation counterbalances substrate accessibility regulation
- 47 - Regulation of decomposition by bacterial density is more acute for oligotrophs

48 1. Introduction

49 Organic carbon is involved in most ecological functions provided by soils (Bünemann et al.,
 50 2018). Its cycling in soil depends upon the activity of microorganisms. Soluble organic
 51 molecules are taken up as substrates by specific populations of soil bacteria, and degraded
 52 inside the cells by endoenzymes to provide carbon and energy. This is precisely the case for
 53 the 2,4-Dichlorophenoxyacetic acid (2,4-D) used in this study as a generic model compound
 54 (Don and Weightman, 1985; Pieper et al., 1988; Boivin et al., 2005). Bacterial degradation of
 55 soil carbon has generally been modeled with the Monod equation, where the specific
 56 substrate uptake rate is controlled by substrate concentration and bacterial traits such as
 57 the maximum specific growth rate, the yield (or carbon use efficiency) and the “maximum

58 specific uptake efficiency” (e.g. Monod, 1949; Sinton et al., 1986; Cheyns et al., 2010). With
59 the Monod equation, at the lowest substrate concentration, the specific uptake rate is
60 linearly proportional to the substrate concentration. The proportionality factor is referred to
61 here as the “maximum uptake efficiency” and it reflects the maximal ability of the cell to
62 capture substrate molecules that collide with its membrane (Button, 1978, 1983). The
63 maximum uptake efficiency can also be understood as the volume from which a cell can
64 harvest substrate per unit of time, as used in some studies (Desmond-Le Quéméner and
65 Bouchez, 2014; Nunan et al., 2020; Ugalde-Salas et al., 2020). Each bacterium is assumed to
66 be exposed to the whole substrate concentration of its surroundings, without any limitation
67 by the population density (Lobry and Harmand, 2006).

68 The direct contact (exposure) between bacteria and substrate depends on their spatial
69 distributions (Holden and Firestone, 1997; Nunan et al., 2007). Bacteria and substrate are
70 both heterogeneously distributed as a result of numerous biotic and abiotic processes
71 (Dechesne et al., 2014; Kuzyakov and Blagodatskaya, 2015). There are complex feedback
72 loops between these distributions, dispersive transport processes such as diffusion and
73 hydrodynamic dispersion (Madsen and Alexander, 1982; Breitenbeck et al., 1988), and the
74 bacterial activity itself such as consumption and growth (Poll et al., 2006).

75 Aggregated bacterial distributions, as observed at the mm-scale for 2,4-D degraders (Vieublé
76 Gonod et al., 2003), have been shown to decrease degradation rates when the distribution
77 of substrate is homogeneous, because of local substrate depletion (Pallud et al., 2004;
78 Dechesne et al., 2010). Yet, the role of bacterial metabolic traits on the impact of bacterial
79 and substrate distributions on degradation remains mostly unknown, especially when
80 substrate and bacteria are heterogeneously and dynamically redistributed in soils over

81 μm -to-cm scales by numerous spatial disturbances (Madsen and Alexander, 1982;
82 Breitenbeck et al., 1988; König et al., 2020). We investigated the extent to which bacterial
83 activity and transport processes can be treated independently or should be integrated to
84 characterize, understand and predict degradation under various advective, diffusive and
85 dispersive conditions. The simultaneous characterization of the impacts of bacterial traits
86 and transport parameters through their mutual interactions is methodologically challenging.
87 It requires several well-controlled experiments in comparable degradation conditions, with
88 specific spatial distributions of substrate and degraders in specific transport conditions, and
89 a spatiotemporal monitoring of the different carbon pools.

90 Among the scarce relevant datasets (e.g. Dechesne et al., 2010), we used the two sets of
91 cm-scale soil-core experiments performed by Pinheiro et al. (2015, 2018), in which the
92 degradation of 2,4-D under different initial spatial distributions and transport conditions was
93 measured in similar repacked soil columns. Mostly reported independently, they have shown
94 first that the proximity between bacteria and the initial location of a heterogeneously
95 distributed substrate exerts a strong control on mineralization. Mineralization was greater
96 when bacteria were close to the initial location of substrate, even though most of the initial
97 dissolved substrate diffused away from its initial location. This was attributed to the fact that
98 bacteria located far from the initial substrate location were only exposed to highly diluted
99 substrate concentrations (Babey et al., 2017). However, the hydrodynamic dispersion of
100 both bacteria and substrate away from their initial location caused a greater than four-fold
101 increase in the mineralization of substrate that was not leached out, to the point that it
102 almost reached the same performance as in homogeneous conditions in which there was no
103 dilution (Pinheiro et al., 2018). The surprising increase in mineralization suggests a regulation

104 of mineralization by population density compensating the effect of substrate dilution, the
105 activity of bacteria being enhanced when their density is diluted by the dispersive
106 percolation events. While such regulations by bacterial density have not yet been considered
107 in soils, presumably because of the extremely low apparent bacterial densities found in soils
108 (Young et al., 2008), they are well known in bioreactors, where they are usually modeled by
109 the ratio-dependent Contois growth law (Contois, 1959; Harmand and Godon, 2007).

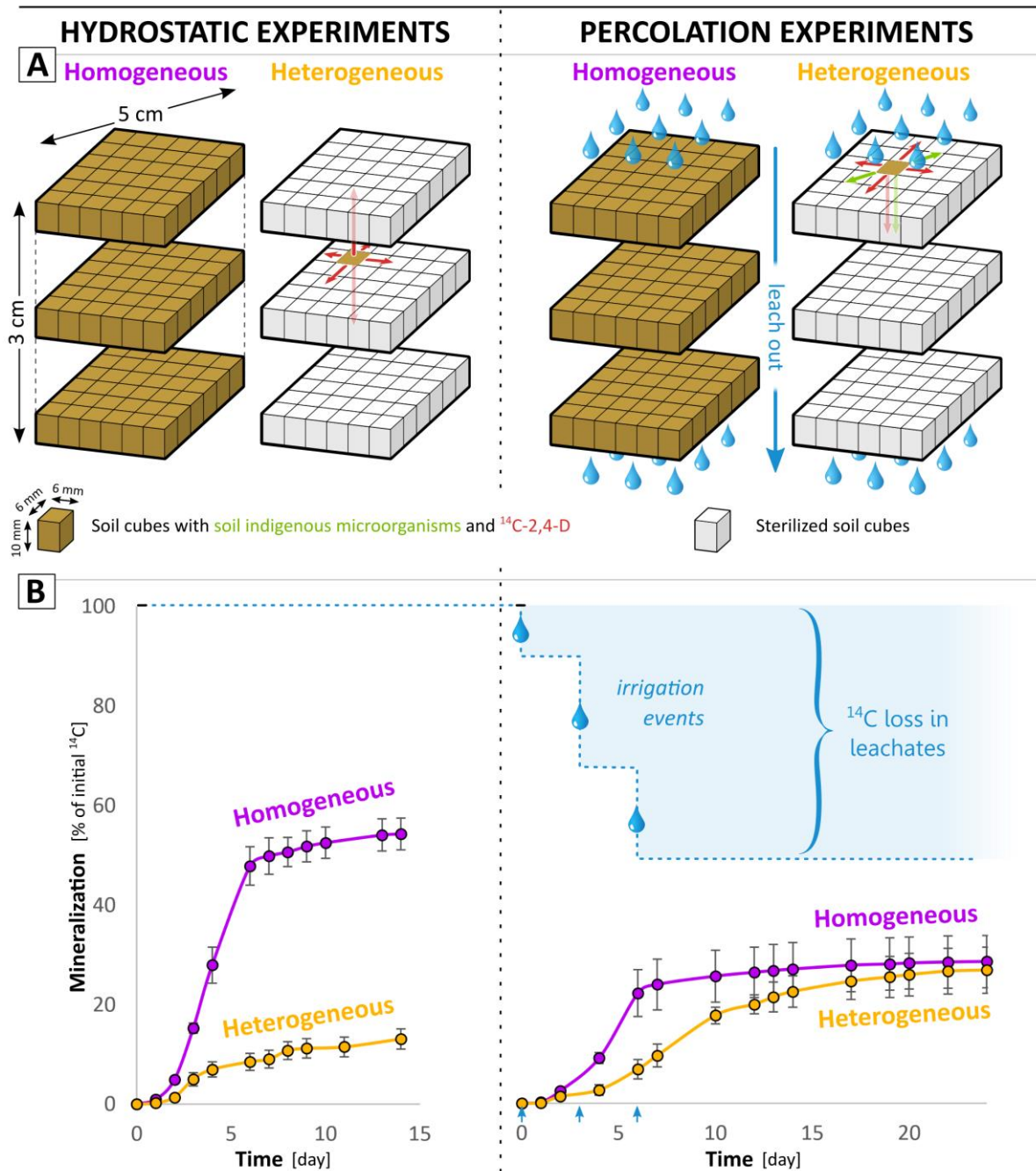
110 In order to determine the relevance of the putative bacterial decomposer density effect on
111 decomposition, we developed a quantitative approach to model the two sets of experiments
112 within the same unified framework (section 2). We assessed the relevance of previously
113 developed models, improved the calibration of a Monod-based model and investigated an
114 alternative Contois-based model (section 3). We discuss the implication of the results on the
115 controlling factors of soil organic carbon cycling, on the relevant bacterial growth models
116 and on the possible bacterial strategies (section 4).

117 **2. Models and methods**

118 ***2.1. Experiment scheme, geometry and initial distributions***

119 We briefly introduce the experiments performed previously and highlight aspects of the
120 experiments that are important for the modeling (Fig. 1). The full experimental setting is
121 presented in the supplementary materials (Fig. S1 and Table S1) for the sake of
122 completeness. Soil columns were packed with two homogeneous or heterogeneous
123 arrangements of soil cubes, either sterilized, or hosting the indigenous microbial
124 communities (referred to as “degraders”) and amended with ¹⁴C-labelled 2,4-D (referred to

125 as “substrate”). Two sets of experiments, referred to as “hydrostatic” and “percolation”
126 conditions, were performed respectively with only substrate diffusion (Pineiro et al., 2015),
127 or with additional substrate and bacterial advection and dispersion caused by water
128 percolation (Pineiro et al., 2018). The initial locations of the bacteria and substrate were
129 set in the model according to the experimental conditions (Fig 1A). Initial concentrations
130 used in the model are detailed in Table 1. In the experiments, the mass of mineralized ^{14}C
131 derived from the degradation of the labelled 2,4-D was monitored at the core scale during
132 at least two weeks (**Fig. 1B**). These data were used to confront the model processes with a
133 physical system, as detailed in section 2.5.



134

135 **Fig. 1.** Model experimental design, geometry and initial distributions (A) based on previously
 136 performed experiments in hydrostatic (Pineiro et al., 2015) and percolation (Pineiro et al.,
 137 2018) conditions. The red and green arrows refer respectively to the 2,4-D and degrader
 138 modeled displacements. (B) Experimental cumulated production of CO₂ (adapted from
 139 Pineiro et al. (2015, 2018), permission for reproduction granted by Elsevier).

140 **2.2. Bioreactive model**

141 The bioreactive model extends the model published by Babey et al. (2017) (Fig. 2) to account
 142 for Contois growth law as an alternative to Monod's. The sorption processes, the bacterial
 143 lag phase and the biomass recycling described below were previously discussed and their
 144 use justified in Babey et al. (2017) to consistently represent the experimental data. The $r(\cdot)$
 145 notation expresses the reaction rates of the biochemical dynamics that are expressed as
 146 follows:

$$r(S) = k_{AS} A - k_{SA} S - k_R S - \frac{\mu}{y} B + m_t \chi B \quad (1)$$

$$r(A) = k_{SA} S - k_{AS} A \quad (2)$$

$$r(R_S) = k_R S \quad (3)$$

$$r(CO_2) = \frac{(1-y)}{y} \mu B \quad (4)$$

$$r(B) = \mu B - m_t B \quad (5)$$

$$r(R_B) = m_t (1 - \chi) B \quad (6)$$

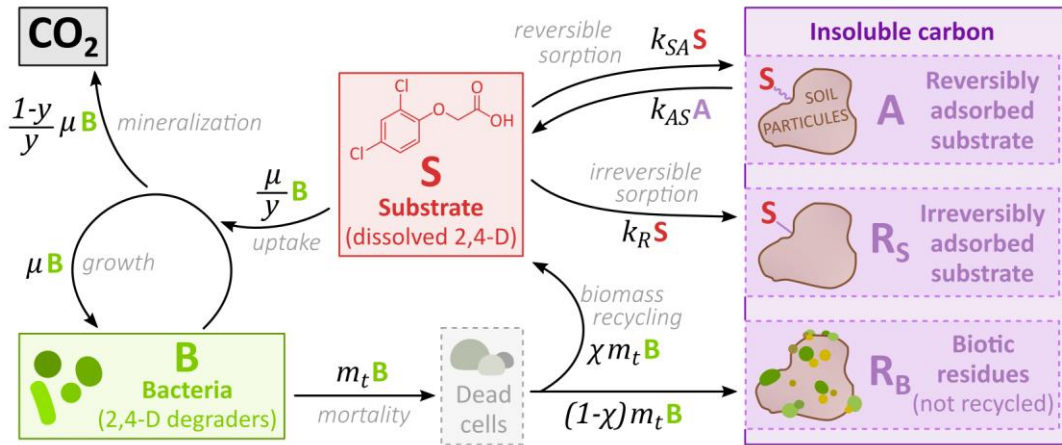
147 All variable and parameter definitions are listed in Table 1. The dynamics of the specific
 148 growth rate μ are given, for the Monod-based model, by:

$$\frac{\partial \mu}{\partial t} = \alpha \left(\mu_{max} \frac{S}{\kappa_M + S} - \mu \right) \quad (7)$$

149 and, for the Contois-based model, by:

$$\frac{\partial \mu}{\partial t} = \alpha \left(\mu_{max} \frac{S/B}{\kappa_C + S/B} - \mu \right) = \alpha \left(\mu_{max} \frac{S}{\kappa_C B + S} - \mu \right) \quad (8)$$

150 where $\mu = 0$ at $t = 0$.



151
 152 **Fig. 2.** Graphical representation of the biochemical model and carbon fluxes identified by the
 153 arrows. Under low substrate concentrations S , the specific uptake rate $(1/y) \cdot \mu$ becomes
 154 equal to $S \cdot (1/y) \cdot \mu_{max} / K_M$, where $(1/y) \cdot \mu_{max} / K_M$ is referred to as the “maximum specific
 155 uptake efficiency”.

156 **Table 1.**

157 Values and range of values of the reactive transport model. The effective dispersion
 158 coefficient d_{disp} applies only to heterogeneous percolation experiments. $B(t = 0)$ is the initial
 159 density of bacteria in the natural cubes. It is considered 1.6 times smaller in the percolation
 160 experiments than in the hydrostatic experiments according to the initial experimental
 161 measurements.

| Parameter description | Symbol | Unit | Fixed values and admissible ranges for screening |
|-------------------------------------|------------|---|--|
| Initial substrate concentration | $S(t = 0)$ | $\mu\text{g} \cdot \text{g}^{-1}$ (mass of substrate carbon per mass of dry soil) | 0.825 ^b |
| | | $\mu\text{g} \cdot \text{g}^{-1}$ | 6.52 ^b |
| Reversible adsorption coefficient | k_{SA} | d^{-1} | 0.09207 |
| Reversible desorption coefficient | k_{AS} | d^{-1} | 4.361 |
| Irreversible adsorption coefficient | k_c | d^{-1} | 0.01296 |

| | | | | |
|--|---------------------------|---|--|--------------------------------|
| Uptake yield | | y | - | 0.5206 |
| Maximum specific uptake rate | | $(1/y) \cdot \mu_{max}$ | d^{-1} | [0.0190 – 19.5] |
| Specific uptake efficiency at the lowest substrate concentration | | $(1/y) \cdot \mu_{max} / \kappa^a$ <i>where κ is κ_M or $B(t=0) \cdot \kappa_C$</i> | $g \cdot \mu g^{-1} \cdot d^{-1}$ (mass of dry soil per mass of bacterial carbon per unit of time) | [0.0152 – 159] ^c |
| Accommodation rate | | α | d^{-1} | [0.00934 – 934] |
| Initial degrader population density | Hydrostatic experiments | $B(t=0)$ | $\mu g \cdot g^{-1}$ (mass of bacterial carbon per mass of dry soil) | [0.0161 – 1.61] ^d |
| | Percolation experiments | $B(t=0)$ | $\mu g \cdot g^{-1}$ | [0.0101 – 1.01] ^d |
| Mortality rate | | m_t | d^{-1} | 0.0602 |
| Biomass recycling yield | | χ | - | 0.6010 |
| Effective diffusion coefficient | | d_{diff} | $m^2 \cdot d^{-1}$ | $1 \cdot 10^{-5}$ ^e |
| Effective dispersion coefficient | | d_{disp} | $m^2 \cdot d^{-1}$ | [0 – ∞] |
| Leaching rates (days 0; 3; 6) | Homogeneous experiments | v | - | 0.108; 0.226; 0.180 |
| | Heterogeneous experiments | | | 0.107; 0.223; 0.178 |

162 ^a The half-saturation constant κ corresponds to κ_M for the Monod-based model and
163 $B(t=0) \cdot \kappa_C$ for the Contois-based model (where $B(t=0)$ is the value from the hydrostatic
164 experiments).

165 ^b The initial substrate concentration $S(t=0)$ is set equal to the ¹⁴C-2,4-D concentration
166 amended in the experiments.

167 ^c The values of $(1/y) \cdot \mu_{max} / \kappa$ correspond to ranges of $[1.65 - 1.73 \cdot 10^4]$ $l \cdot g^{-1} \cdot d^{-1}$ (volume of
168 water per mass of bacteria per unit of time)

169 ^d The values of $B(t=0)$ correspond respectively to ranges of $[1.48 \cdot 10^{-4} - 1.48 \cdot 10^{-2}]$ $g \cdot l^{-1}$ (mass
170 of bacteria per volume of water) for the hydrostatic experiments and $[9.24 \cdot 10^{-5} - 9.24$
171 $\cdot 10^{-3}]$ $g \cdot l^{-1}$ for the percolation experiments.

172 ^e The value of d_{diff} has been calibrated on a $3 \times 6 \times 6$ grid in similar conditions (Babey et al.,
173 2017).

174 The dissolved substrate S is either reversibly adsorbed to soil particles (pool A) or irreversibly
175 adsorbed (pool R_S) (Eqs. (1), (2), (3)), or taken up by bacteria B (Eq. (1)) and metabolized into
176 CO_2 (Eq. (4)) and new biomass B (Eq. (5)). k_{SA} and k_{AS} are the reversible sorption coefficients.
177 k_R is the irreversible one. Bacteria death occurs at a constant rate m_t (Eq. (5)) and a fraction
178 of the bacterial necromass is considered to return to the dissolved substrate pool S to
179 account for biomass recycling (Eq. (1)), while the rest is transformed to biotic residues R_B
180 (Eq. (6)). The remobilization of carbon previously absorbed by bacteria is necessary to
181 adequately predict the slower dynamics of mineralization that takes place once most of the
182 dissolved substrate has been consumed, observed after 5 days in homogeneous experiments
183 and after respectively 3 or 10 days in the heterogeneous hydrostatic or percolation
184 experiments. This remobilization is modeled in the form of a biomass recycling in order to
185 be consistent with the model previously published in Babey et al. (2017), but similar effects
186 could be achieved by other mechanisms, like a slower mineralization of biogenic residues
187 (Fig. S9). Its impact on the final mineralization does not account for more than 10% of the
188 substrate that is not leached out. The adsorbed substrate and biotic residues form the pool
189 of insoluble carbon $A + R_S + R_B$. The substrate S is consumed by bacteria B according to their
190 specific uptake rate $(1/y) \cdot \mu$ expressed either by the substrate-dependent Monod growth law
191 (Eq. (7)) (Monod, 1949) or by the ratio-dependent Contois growth law (Eq. (8)) (Contois,
192 1959). The yield coefficient y relates the specific uptake rate $(1/y) \cdot \mu$ to the specific growth
193 rate μ . μ_{max} is the maximum specific growth rate. K_M and K_C are Monod and Contois constants
194 respectively. The effective uptake is delayed by the accommodation rate α , which explicitly
195 takes into account the “memory” effects of the bacteria when adapting to new conditions
196 (Patarinska et al., 2000). This delay is necessary to capture the mineralization lag time at the
197 beginning of the experiments (see Fig. S10). Over long time periods ($t \gg 1/\alpha$), μ follows the

198 exact expression of the Monod or Contois equations. All modeled pools (S , B , CO_2 , A , R_S and
199 R_B) were expressed as carbon concentrations in $\mu\text{g}\cdot\text{g}^{-1}$ (mass of carbon per mass of dry soil)
200 considering a soil water content of $0.205\text{ g}\cdot\text{g}^{-1}$ (mass of water per mass of dry soil), a bulk
201 density of the soil column of $1.3\ 10^3\text{ g}\cdot\text{l}^{-1}$ (mass of dry soil per apparent soil volume) and an
202 average bacterial dry weight of $2.8\ 10^{-13}\text{ g}$ corresponding to $1.49\ 10^{-13}\text{ g}$ of carbon per cell.
203 These values of water content and bulk density were those set up in the experiments, the
204 latter corresponding to a water potential adjusted at -31.6 kPa (pF 2.5). The average bacterial
205 weight was assumed based on Dechesne et al. (2010) and Pinheiro et al. (2015). The water-
206 filled pore space (54%, volume of water per volume of pores) was such that oxygen was not
207 considered a limiting factor for 2,4-D degradation.

208 ***2.3. Reactive transport model***

209 The transport model is based on the substrate diffusion model of Babey et al. (2017) to which
210 advective-dispersive processes explored in the experiments of Pinheiro et al. (2018) are
211 added. Hydrodynamic leaching out and dispersion of bacteria and substrate were observed
212 in the percolation experiments while the substrate was reported to diffuse in all
213 experiments. Hydrodynamic leaching and dispersion were modeled independently, as they
214 result from, respectively, bypass flow through large pores and complex hydrodynamic
215 dispersion processes coming not only from usual flow mechanisms but also from large
216 saturation variations and local redistribution of moisture in the pore network. Due to the
217 lack of adequate experimental data to characterize the details of the dispersion process, we
218 applied a simple isotropic dispersion coefficient. Complementary numerical simulations
219 show that other anisotropic dispersion parameterizations are only weakly sensitive (Fig. S3

220 and S4). Bacterial and substrate transports by percolation were described with the same
 221 advective and dispersive parameters. This assumption did not significantly alter the results
 222 (Fig. S5 and S6). Coupled to the equations of the bioreactive model ((1)-(8)), the full reactive
 223 transport model is given by:

$$\frac{\partial S}{\partial t} = r(S) + \nabla(d_{diff} \nabla S) + G(\nabla(d_{disp} \nabla S) - \nu S) \quad (9)$$

$$\frac{\partial B}{\partial t} = r(B) + G(\nabla(d_{disp} \nabla B) - \nu B) \quad (10)$$

$$\frac{\partial U}{\partial t} = r(U) \quad \text{for } U = A, R_B, R_S \text{ and } CO_2 \quad (11)$$

224 where d_{diff} is the effective molecular diffusion coefficient of S , d_{disp} is the effective
 225 hydrodynamic dispersion coefficient of S and B and ν is their leaching rate. Note that the
 226 dispersion coefficient d_{disp} mostly affected the spreading of bacteria, given that substrate
 227 was mainly spread by diffusion, as confirmed by consistent results from equivalent models
 228 without hydrodynamic dispersion of S (Fig. S7 and S8). Effective diffusion and dispersion
 229 processes were assumed to be isotropic and uniform at the column-scale. Dispersion and
 230 leaching were active only during the observed 1-hour percolation events at days 0, 3 and 6
 231 as controlled by the function G defined as:

$$G(t) = 1 \quad \text{for } t = [0d - 0d1h]; [3d - 3d1h]; [6d - 6d1h] \quad (12)$$

$$G(t) = 0 \quad \text{otherwise.}$$

232 No-flow boundary conditions were imposed at the edges of the soil core ($\nabla S = 0$ and $\nabla B = 0$)
 233 during periods outside of the percolation events. The transient evolutions of the water
 234 content and their effects on concentrations were not considered because of the short

235 duration of the percolation events (1 h) and the absence of detectable effects on the
236 experimental mineralization curve around the percolation events (Fig. 1D). Hydration
237 conditions were considered constant, constrained by the water potential adjusted
238 to -31.6 kPa. No bacterial mobility was observed in the hydrostatic experiments, suggesting
239 that the bacterial mobility observed in the percolation experiments resulted primarily from
240 hydrodynamic dispersion.

241 Carbon pools concentration dynamics were simulated on a $3 \times 6 \times 6$ regular mesh grid.
242 Although the shape of the grid was slightly different from that of the cylindrical soil-core, it
243 did not have any observable impact (Babey et al., 2017). We recall that substrate and
244 bacteria were initially co-located in the same cube(s). Each cube was considered to be
245 physically, chemically and biologically homogeneous. Diffusion and dispersion were
246 simulated using a finite-difference scheme (Iserles, 2009) and coupled with the bioreactive
247 model, itself solved by the 4th order Runge-Kutta integration method function of MATLAB
248 (Shampine and Reichelt, 1997). The coupling of transport and bioreactive models was
249 achieved with a sequential non-iterative operator-splitting method, in which the equations
250 are resolved within each time step in a sequence of one transport step followed by one
251 bioreactive step (Carrayrou et al., 2004; Lagneau and van der Lee, 2010). The time steps were
252 smaller than the characteristic diffusion and reaction times to avoid any coupling issues.

253 ***2.4. Exploratory screening***

254 Parameters and their values are listed in Table 1. Sorption parameters and the diffusion
255 coefficient were set at values that were calibrated and validated by Babey et al. (2017) in
256 independent experiments without degradation. The mortality rate and the biomass recycling

257 yield were also kept at the values calibrated in Babey et al. (2017) as they were considered
258 to be well constrained by the residual mineralization dynamics of the homogeneous
259 hydrostatic experiment (Fig. 1D). The four biological parameters primarily involved in the
260 biological response of bacteria to the concentration of substrate were determined to be
261 $(1/y) \cdot \mu_{max}$, α , $B(t=0)$ and either $(1/y) \cdot \mu_{max}/\kappa_M$ for the Monod-based model or
262 $(1/y) \cdot \mu_{max}/(B(t=0) \cdot \kappa_C)$ for the Contois-based model. Each of these four parameters were
263 sampled over 7 logarithmically-distributed values within the theoretically and physically
264 relevant ranges given by Babey et al. (2017), and all possible combinations of values were
265 screened (Table S2). We recall that the maximum specific uptake efficiency $(1/y) \cdot \mu_{max}/\kappa_M$
266 characterizes the bacterial uptake of substrate at the lowest substrate concentration
267 (Button, 1991), while the maximum specific uptake rate $(1/y) \cdot \mu_{max}$ characterizes the
268 bacterial uptake at the highest substrate concentration. Note that the uptake yield y was
269 fixed at the value calibrated by Babey et al. (2017) with a high degree of certainty. The initial
270 maximum uptake efficiency $(1/y) \cdot \mu_{max}/(B(t=0) \cdot \kappa_C)$ in the Contois-based model was
271 screened in the same range as $(1/y) \cdot \mu_{max}/\kappa_M$. The accommodation rate α of the degrader
272 response ranged from a negligible delay of few minutes ($\alpha = 934 \text{ d}^{-1}$) to a prolonged delay of
273 around 10 days ($\alpha = 9.34 \cdot 10^{-2} \text{ d}^{-1}$). $B(t=0)$ values were screened around the initial
274 experimental measurements of the *tfdA* gene copy number, assuming that one *tfdA*
275 sequence corresponded to one bacterium. They ranged over two orders of magnitude to
276 account for the uncertainty of the conversion of *tfdA* copy number into alive 2,4-D degraders
277 (Bælum et al., 2006, 2008). Bacterial density in the uptake efficiency expression will also be
278 expressed in $\text{g} \cdot \text{l}^{-1}$ (mass of bacteria per volume of water) for a more direct comparison with
279 the relevant literature.

280 The spatial distribution of bacteria observed at the end of the experiments could not be used
 281 to determine the effective dispersion coefficient d_{disp} (Fig. S2). While they qualitatively
 282 ascertained that bacteria spread orthogonally to the percolation direction, experimental
 283 data were not sufficiently resolved to be used quantitatively. The dispersion coefficient was
 284 thus screened over 10 values ranging from no dispersion ($d_{disp} = 0$) to complete instant
 285 homogenization of the soil core ($d_{disp} = \text{inf}$) (Table S2). In order to analyze the result of
 286 bacterial dispersion in terms of distance from the initial location of the substrate, we
 287 compute the root-mean-square displacement of bacteria, defined as the root-mean-square
 288 of their spreading during the duration Δt of one percolation event and expressed as
 289 $\sqrt{6 d_{disp} \Delta t}$ (Stana, 2020). The effective diffusion coefficient d_{diff} had been calibrated
 290 independently from percolation conditions (Pinheiro et al., 2015; Babey et al., 2017). The
 291 leaching rates v were determined based on the experimental masses of leached ^{14}C (Pinheiro
 292 et al., 2018) (Table 1). Detailed values for the screened parameters are listed in Table S2.

293 **2.5. Model to data comparison**

294 The comparison between the results of the model and the experimental data was based on
 295 the core-scale data of mineralization deduced from the carbon mass m_{CO_2} of $^{14}\text{CO}_2$ emissions:

$$m_{CO_2}(t) = \int_V CO_2(x, t) dx \quad (13)$$

296 with V the volume of the soil cores. Mineralization at a given time t was expressed as the
 297 carbon mass of cumulated $^{14}\text{CO}_2$ emissions ($m_{CO_2,q}(t)$) per initial carbon mass of
 298 ^{14}C -substrate S ($m_{S,q}(t = 0)$) where the index q identifies the experiment at hand. Indices

299 1, 2, 3 and 4 are respectively given to the homogeneous hydrostatic, heterogeneous
 300 hydrostatic, homogeneous percolation and heterogeneous percolation experiments.
 301 Data-to-model adequacy was assessed for each of the experiments by a classical root-mean-
 302 square evaluation function J_q comparing the modeled mineralization of Eq. (4) to the
 303 measured mineralization at the n_q available sampling times t_i :

$$J_q = \left(\frac{1}{n_q} \sum_{i=1}^{n_q} \left(\frac{m_{CO_2,q}^{mod}(t_i) - m_{CO_2,q}^{data}(t_i)}{m_{S,q}(t=0)} \right)^2 \right)^{\frac{1}{2}} \quad (14)$$

304 Discrepancies over the full set of experiments J_{1234} were thus expressed as:

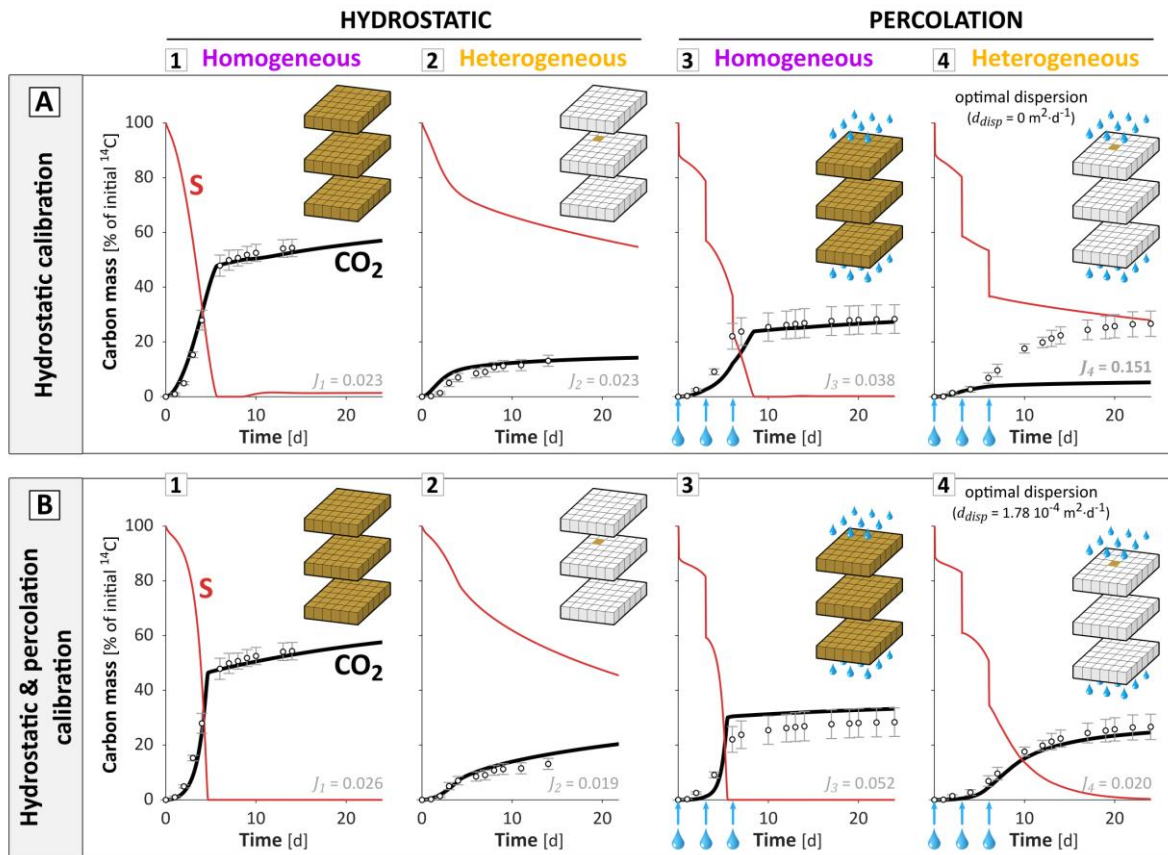
$$J_{1234} = \left(\frac{1}{4} \sum_{k=1}^4 J_k^2 \right)^{\frac{1}{2}} \quad (15)$$

305 Following the systematic parameter screening described in section 2.4, the parameter set
 306 minimizing J_{1234} was determined and referred to as the set calibrated on both hydrostatic
 307 and percolation experiments. The measurement errors were in average 1.7 times higher in
 308 the percolation experiments than in the hydrostatic experiments. This was assumed to be
 309 due to differences in experimental setup between the two sets of experiments of Pinheiro
 310 et al. (2015, 2018). This error difference contributed to limit the weight of the percolation
 311 experiments when determining the best-fitting parameter set over the whole set of
 312 experiments (J_{1234}). We made the choice to give an equal weight to all experiments by only
 313 taking into account the average CO₂ values.

314 **3. Results**

315 **3.1. Model calibration**

316 The calibration of the bioreactive transport model carried out using only the hydrostatic
317 experimental data (Babey et al., 2017) led to a minimal discrepancy between data and model
318 of $J_{12} = 0.023$ (Fig. 3-A1 and A2). This pre-existing parameterization was used to provide blind
319 predictions of the percolation experiments, with the effective dispersion coefficient d_{disp} as
320 an additional fitting parameter. It gave a reasonable prediction of mineralization in the
321 homogeneous percolation experiment ($J_3 = 0.038$, Fig. 3-A3) but failed in the heterogeneous
322 percolation experiment ($J_4 = 0.151$, Fig. 3-A4), regardless of the dispersion coefficient values.
323 The smallest discrepancy J_4 was surprisingly obtained without any bacterial dispersion
324 ($d_{disp} = 0$) in contradiction with the bacterial spread observed in the experimental data
325 (Fig. S2). The final predicted mineralization was highest when bacteria remained aggregated
326 close to the initial location of the substrate. The highest predicted mineralization was
327 however four times lower than the experimental data. The large gap between the
328 experimental data and the modeled scenario suggests that bacterial proximity to the initial
329 substrate location is not the underlying explanatory mechanism for the high mineralization
330 rates. On the contrary, it suggests that mineralization might rather be increased by the
331 dispersion of bacteria towards more diluted substrate concentrations, and that the identified
332 bacterial traits do not match this increase of mineralization with dispersion.



333

334

Fig. 3. Mineralization dynamics predicted with the Monod-based model calibrated on the hydrostatic experiment only (A) and on both hydrostatic and percolation experiments (B).

335

The related experimental setups are indicated in the top right corner of each graph. The

336

agreement between experiments and model is indicated by the value of discrepancy J

337

displayed at the bottom and can be visually assessed by the proximity between the black line

338

and the dots representing respectively the model results and experimental data. The red line

339

refers to the carbon mass of substrate remaining in the soil core. In the percolation

340

experiments (A3,4 and B3,4), around 51% of the initial mass of ^{14}C was lost through leaching

341

after the three percolation events ($t = 0, 3$ and 6 days, blue arrows). The carbon balance

342

among the different pools is detailed in Fig. S11. Note that the reversible sorption eventually

343

accounted for less than 2% of the initial carbon mass and therefore did not significantly alter

344

the results.

345

346

In order to investigate the capacity of the reactive transport model to fit both hydrostatic

347

and percolation experimental data, the biological parameters ($(1/y) \cdot \mu_{max} / \kappa_M$, $(1/y) \cdot \mu_{max}$, α ,

348

$B(t=0)$) and the dispersion coefficient (d_{disp}) were calibrated on both hydrostatic and

349 percolation experiments following the screening approach given in section 2.4 to minimize
350 J_{1234} . The mineralization dynamics were adequately predicted in all four experiments with
351 the biological parameter set giving the lowest overall discrepancy ($J_{1234} = 0.032$) and a
352 non-zero dispersion coefficient ($d_{disp} = 1.78 \cdot 10^{-4} \text{ m}^2 \cdot \text{d}^{-1}$) (Fig. 3 and Table 2). The non-zero
353 dispersion coefficient indicates that the calibrated model accounts for a positive impact of
354 bacterial dispersion on degradation. The model results suggest that this effect is necessary
355 to successfully predict the high degree of degradation in the experimental data. Compared
356 to the parameters calibrated only using the hydrostatic experiments, the parameter set
357 calibrated on both hydrostatic and percolation experiments also displayed a much higher
358 maximum uptake efficiency ($(1/y) \cdot \mu_{max} / \kappa_M = 26.5 \text{ g} \cdot \mu\text{g}^{-1} \cdot \text{d}^{-1}$ (mass of dry soil per mass of
359 bacterial carbon per unit of time) (Table 2). The systematic exploration of the parameter
360 space showed that high maximum uptake efficiency was a common feature of the 1%
361 best-fitting parameterizations over both hydrostatic and percolation experiments (smallest
362 J_{1234}), with values of 159 and $26.5 \text{ g} \cdot \mu\text{g}^{-1} \cdot \text{d}^{-1}$, corresponding respectively to $1.73 \cdot 10^4$ and
363 $2.89 \cdot 10^3 \text{ l} \cdot \text{g}^{-1} \cdot \text{d}^{-1}$ (volume of water per mass of bacteria per unit of time). It underlines the
364 essential role of the maximum uptake efficiency for modulating the impact of dispersion on
365 degradation, further detailed and explained in section 3.2.3.

366 **Table 2.**

367 Parameters for the Monod-based model calibrated by the screening approach (section 2.2)
368 on the hydrostatic experiments only (Babey et al., 2017) and on both hydrostatic and
369 percolation experiments, and for the Contois-based model calibrated on both hydrostatic
370 and percolation experiments, as described in section 2.4

| Parameter symbol | Unit | Monod model calibration | | Contois model calibration | |
|----------------------------------|--|--|---|---|-----------------------|
| | | on the sole hydrostatic experiments | on both hydrostatic & percolation experiments | on both hydrostatic & percolation experiments | |
| $(1/y) \cdot \mu_{max}$ | d ⁻¹ | 1.22 | 9.73 | 4.86 | |
| $(1/y) \cdot \mu_{max}/\kappa^a$ | g·μg ⁻¹ ·d ⁻¹ (mass of dry soil per mass of bacterial carbon per unit of time) | 2.65 ^b | 26.5 ^b | 2.65 ^b | |
| α | d ⁻¹ | 9.341 10 ⁻¹ | 9.34 10 ⁻² | 9.34 10 ⁻² | |
| $B(t = 0)$ | Hydrostatic experiments | μg·g ⁻¹ (mass of bacterial carbon per mass of dry soil) | 1.61 10 ⁻¹ | 3.23 10 ⁻² | 3.76 10 ⁻¹ |
| | Percolation experiments | μg·g ⁻¹ | 1.01 10 ⁻¹ | 2.01 10 ⁻² | 2.34 10 ⁻¹ |
| d_{disp} | m ² ·d ⁻¹ | 0 ^c | 1.78 10 ^{-4 c} | 10 ^{-5 c} | |
| J_{1234} | - | 0.079 | 0.032 | 0.022 | |

371 ^a The half-saturation constant κ corresponds to κ_M for the Monod-based model and
372 $B(t = 0) \cdot \kappa_C$ for the Contois-based model (where $B(t = 0)$ is the value from the hydrostatic
373 experiments).

374 ^b Values of $(1/y) \cdot \mu_{max}/\kappa$ correspond respectively to 2.89 10², 2.89 10³ and 2.89 10² l·g⁻¹·d⁻¹
375 (volume of water per mass of bacteria per unit of time).

376 ^c The corresponding spreading values induced by the hydrodynamic dispersion
377 (root-mean-square displacements) for each percolation events are respectively 0, 6.7 and
378 1.6 mm, to be compared to the 25 mm radius of the soil column.

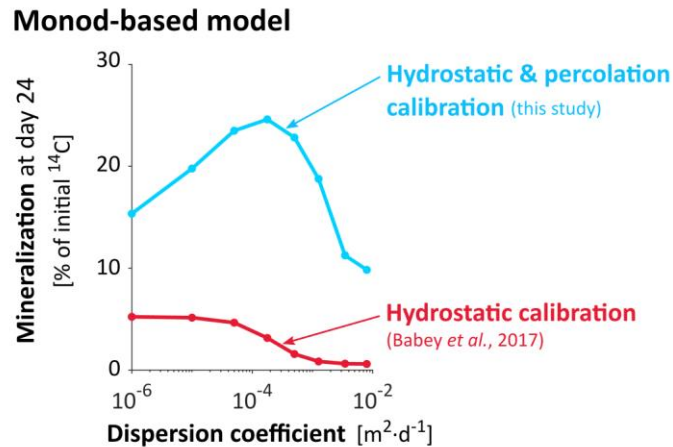
379 **3.2. Analysis of the controls exerted on degradation by substrate dilution and** 380 **bacterial density**

381 The effect of dispersion on degradation differed greatly between the two calibrated sets of
382 biological parameters described in section 3.1. We therefore conducted a more systematic

383 investigation of the coupled impact of bacterial dispersion and bacterial traits on
384 degradation, revealing its control by substrate dilution and bacterial density.

385 3.2.1 Impact of dispersion on degradation

386 We used the mineralization at the end of the experimental time (day 24) as a proxy for
387 degradation and determined its sensitivity to dispersion, as a function of the
388 parameterization of bacterial traits. Fig. 4 shows the impact of the dispersion coefficient d_{disp}
389 on the final predicted mineralization for the two calibrated biological parameter sets, all
390 other parameters being kept constant (thick red and blue lines). For the biological parameter
391 set calibrated on hydrostatic experiments, the final mineralization decreased monotonically
392 with dispersion (Fig. 4, red line). For the parameter set calibrated on both hydrostatic and
393 percolation experiments, the final mineralization first increased, reached a maximum around
394 $d_{disp} \approx 10^{-4} \text{ m}^2 \cdot \text{d}^{-1}$ and then decreased (Fig. 4, blue line). These two kinds of behaviors were
395 observed regardless of the parameters α , $(1/y) \cdot \mu_{max}$ and $B(t=0)$ as long as $(1/y) \cdot \mu_{max} / \kappa M$
396 remained the same (Fig. S12). The non-monotonic impact of dispersion on degradation
397 highlights the existence of an optimal bacterial dispersion for which mineralization is the
398 highest. The comparison between the red and blue lines on Fig. 4 suggests that the optimal
399 dispersion value depends on the bacterial uptake efficiency. Note that, although the optimal
400 dispersion value varied with time due to the spatial dynamics of both bacteria and substrate
401 (Fig. S14), it tended towards a limit that was mostly reached within 4 to 7 days and is thus
402 represented at day 24 on Fig. 4.



403
 404 **Fig. 4.** Influence of the dispersion coefficient d_{disp} on mineralization predicted at day 24
 405 $m_{CO_2}(t = 24)$ for the biological parameter set calibrated on the sole hydrostatic experiments
 406 (A, thick red line) and on both hydrostatic and percolation experiments (B, thick blue line).
 407 Note that for the model calibrated on both hydrostatic and percolation experiments, the
 408 value of d_{disp} leading to the highest final mineralization ($d_{disp} = 1.78 \cdot 10^{-4} m^2 \cdot d^{-1}$, thick blue
 409 line) is also equal to its calibrated value leading to the best adequacy with mineralization
 410 kinetics (Table 2). Note that the optimal dispersion value remains the same when
 411 representing the remaining dissolved substrate instead of the mineralization (Fig. S13).

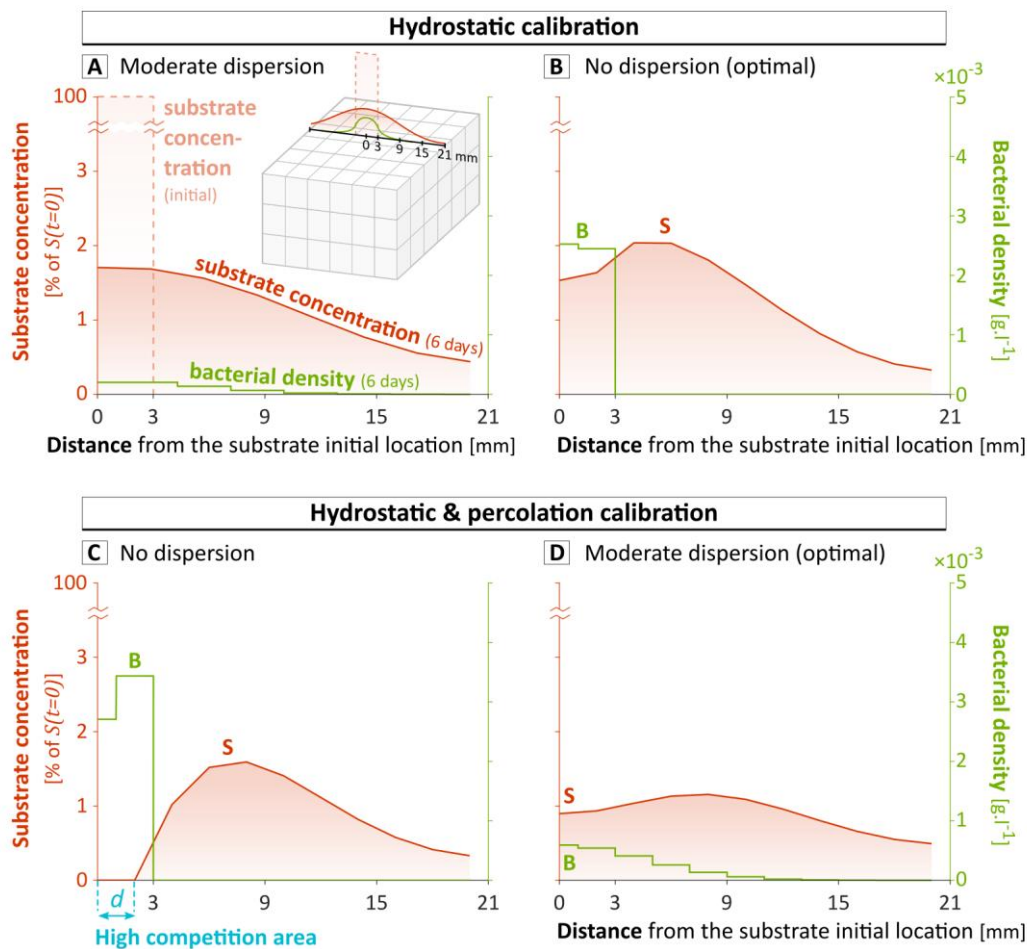
412 3.2.2 Double control of degradation by substrate dilution and bacterial density

413 The non-monotonic effect of bacterial dispersion on degradation is an unusual and key
 414 feature of the model calibrated on both hydrostatic and percolation experiments. In the
 415 following we will present an explanation for how such relationships between dispersion and
 416 degradation could arise, resulting from a non-monotonic spatial substrate profile, itself
 417 derived from the respective effects of substrate dilution and bacterial density.

418 In the model, the instant exposure of bacteria to their substrate is maximal if all the bacteria
 419 are located inside the voxel(s) with the highest substrate concentration. In the hydrostatic
 420 calibrated parameter set, the profile of substrate concentration primarily resulted from its
 421 initial heterogeneity (bell-shape red curve on Fig. 5A and pseudo bell-shape red curve on

422 Fig. 5B). The flux of substrate reaching each bacterium was therefore mostly determined by
423 the distance between the bacterium and the initial location of substrate. The exposure of a
424 single bacterium to the substrate decreased with its distance from the substrate initial
425 location. This effect is referred to as “substrate dilution”. In these cases (Fig. 5A and B),
426 mineralization was mainly regulated by substrate dilution, and therefore reduced by
427 bacterial dispersion (Fig. 4, blue line). However, for the parameter set calibrated on both
428 hydrostatic and percolation experiments, local degradation by aggregated bacteria reshaped
429 the substrate spatial profile, thus critically changing the voxel(s) with the highest substrate
430 concentration. The bacteria aggregated at their initial location consumed the substrate much
431 faster than it was replenished by backward diffusion and dispersion, creating a critical
432 inversion of the substrate gradient, which led to an intra-population competition for
433 substrate (Fig. 5C). The competition was critical for bacterial densities as small as $3.5 \cdot 10^{-3}$
434 $\text{g}\cdot\text{l}^{-1}$ (Fig. 5C). In contrast, the dispersion of bacteria reduced competition by diluting the
435 highest bacterial densities, thus flattening the substrate gradient inversion induced by
436 bacterial local degradation, resulting in a better overall exposure of bacteria to the substrate
437 concentrations, and thus an enhanced mineralization (Fig. 5D). In these cases (Fig. 5C and D),
438 mineralization was mainly regulated by bacterial density, or in other words by the distances
439 among bacteria. The relationship between bacterial density and the limitation of their
440 exposure to the substrate is not instantaneous and is mediated by the local depletion of the
441 substrate concentration. This is expressed in the model equations through the dependence
442 of bacterial activity $\mu(t)$ on substrate concentration $S(t)$ (Eq. (7)) and the dependence of the
443 substrate concentration $S(t)$ on degradation $\mu(t)\cdot B(t)$ (Eq. (1)), within each voxel. However,
444 when bacterial dispersion was too great, substrate dilution became the dominant control
445 again. This suggests that an optimal bacterial spatial spread exists for which the dilution of

446 substrate is compensated by the dilution of high local bacterial densities. The modeled
 447 scenario illustrated by the two calibrated parameter sets were also observed for most of the
 448 other parameter sets. The optimal dispersion coefficient for the 300 best-fitting
 449 parameterizations to both hydrostatic and percolation experiments (smallest J_{1234} values)
 450 was on average $d_{disp} \approx 2 \cdot 10^{-5} \text{ m}^2 \cdot \text{d}^{-1}$ (Fig. S15), corresponding to a root-mean-square
 451 displacement of bacteria of 2.2 mm during each percolation event.



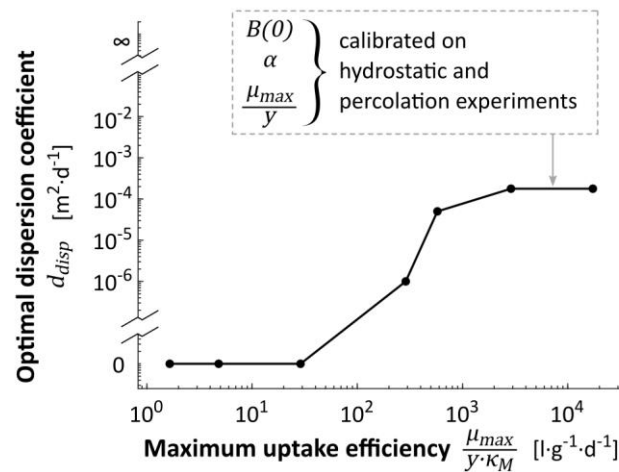
452
 453 **Fig. 5.** Predicted substrate and bacterial spatial concentration profiles after 6 days of
 454 diffusion and dispersion in the conditions of heterogeneous percolation experiment, in
 455 which bacteria and substrate are initially located exclusively in the central cube (from 0 to
 456 3 mm). Results are simulated on a $9 \times 18 \times 18$ grid obtained by subdividing the $3 \times 6 \times 6$ grid
 457 used for the screenings. The results are represented for the parameter set calibrated using
 458 only the sole hydrostatic experiment, either with a moderate dispersion ($d_{disp} = 1.78 \cdot 10^{-4}$
 459 $\text{m}^2 \cdot \text{d}^{-1}$) (A) or with the calibrated dispersion (no dispersion) (B), and for the biological

460 parameter set calibrated on both hydrostatic and percolation experiments, either without
461 dispersion (C) or with the calibrated dispersion ($d_{disp} = 1.78 \cdot 10^{-4} \text{ m}^2 \cdot \text{d}^{-1}$) (D). On one hand,
462 bacteria are exposed to smaller substrate concentrations if they are far from the source
463 (right part of the substrate concentration profiles). On the other hand, bacteria undergo
464 competition if they are too close from each other (left part of the substrate concentration
465 profiles). In (C), the bacteria aggregated below d consume the substrate faster than it is
466 replenished by backward diffusion and dispersion. The total number of bacteria within the
467 whole soil column at day 6 is similar in (A), (B), (C) and (D), respectively equal to $6.0 \cdot 10^5$,
468 $9.5 \cdot 10^5$, $11.5 \cdot 10^5$ and $11.3 \cdot 10^5$. The final mineralization at day 24 is however strongly different
469 between scenario, reaching respectively 3.2%, 5.3%, 9.1% and 24.7% of the initial mass of
470 ^{14}C .

471 3.2.3 *Effect of bacterial uptake efficiency on the impact of dispersion on degradation*

472 A non-monotonic substrate concentration profile only occurs when bacterial degradation
473 locally depletes the substrate faster than it is replenished by diffusion. This area of high local
474 competition for substrate results from either high local densities of bacteria or high
475 competitiveness or both. Bacterial competitiveness is related to their maximum uptake
476 efficiency $(1/y) \cdot \mu_{max}/K_M$, which also describes their capacity to maintain their activity and
477 growth under dilute substrate concentrations (Healey, 1980; Button, 1991; Lobry et al.,
478 1992). Bacteria with high maximum uptake efficiency are thus expected to benefit more
479 from dispersion. Fig. 6 shows the optimal dispersion coefficient as a function of the
480 maximum uptake efficiency, with all other parameters equal to those of the model calibrated
481 on both hydrostatic and percolation experiments. The optimal dispersion coefficient,
482 defined as the dispersion coefficient maximizing the final mineralization, increased with the
483 maximum uptake efficiency. For small maximum uptake efficiencies of $30 \text{ l} \cdot \text{g}^{-1} \cdot \text{d}^{-1}$ and below,
484 mineralization was highest in the absence of dispersion, suggesting a regulation dominated
485 by substrate dilution. For larger maximum uptake efficiencies, dispersion impacted positively

486 mineralization, suggesting that degradation shifted from being regulated by substrate
 487 dilution to being regulated by bacterial densities, as bacteria were both more prone to
 488 competition between themselves and more efficient under diluted substrate conditions. In
 489 other words, the proximity to other bacteria constrained activity more than the proximity to
 490 the substrate initial location enhanced it. This combined effect of the maximum uptake
 491 efficiency and the bacterial dispersion on degradation was a general relationship common
 492 to all parameterizations (Fig. S16).



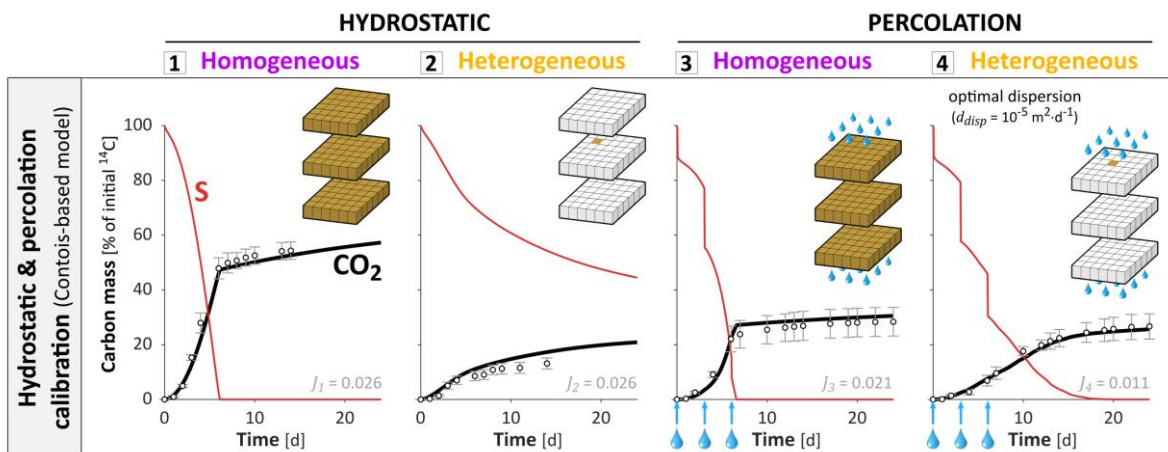
493
 494 **Fig. 6.** Dispersion coefficient giving the highest predicted mineralization at day 24 as a
 495 function of maximum uptake efficiency, all other parameters equal to those of the model
 496 calibrated on both hydrostatic and percolation experiments.

497 **3.3. The Contois-based model as an alternative to Monod**

498 Given that degradation is regulated by both substrate dilution and bacterial density, and that
 499 their relative importance is modulated by bacterial uptake efficiency at the lowest substrate
 500 concentration, $(1/y) \cdot \mu_{max}/K_M$, we investigated the relevance of the Contois model by
 501 applying the calibration methodology of section 2.5, as used in section 3.1. The interest in
 502 the Contois growth law (Eq. (8)) stems from the inclusion of a regulation by density in the

503 expression of the uptake efficiency at the lowest substrate concentration, becoming
 504 $(1/y) \cdot \mu_{max} / (B(t) \cdot \kappa_C)$.

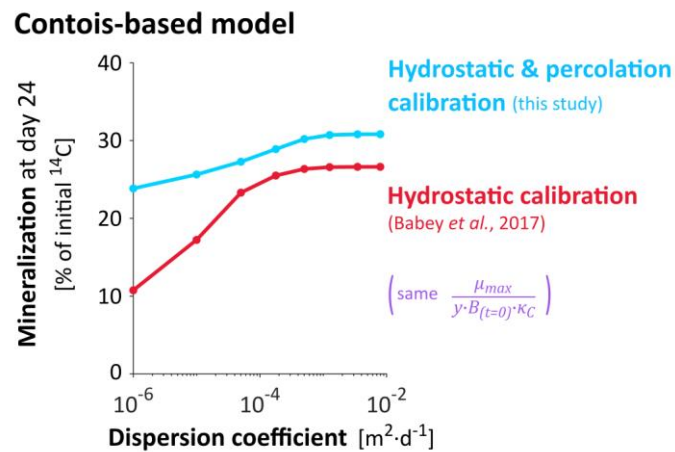
505 In comparison with the Monod-based model, the predictions of the experimental
 506 observations of Pinheiro et al. (2015, 2018) were facilitated with the Contois-based model,
 507 on three levels. First, the Contois-based model captured the degradation dynamics better
 508 than the Monod-based model, especially for the 1% best-fitting parameterizations (smallest
 509 J_{1234} values) (Fig. S17). The calibrated Contois-based model had an overall discrepancy of
 510 $J_{1234} = 0.022$ (Fig. 7), which was smaller than the lowest value of $J_{1234} = 0.032$ obtained for
 511 the calibrated Monod-based model (Fig. 3).



512
 513 **Fig. 7.** Mineralization dynamics predicted with the Contois-based model calibrated on both
 514 hydrostatic and percolation experiments. For representation and legend, see Fig. 3. The
 515 carbon balance among the different pools is detailed in Fig. S11.

516 Second, the parameter sets that fitted homogeneous experiments also performed well
 517 under heterogeneous conditions, as long as the dispersion coefficient d_{disp} was calibrated as
 518 well (Fig. S18). It is an important advantage as it confers a better capacity to predict
 519 degradation kinetics for heterogeneous and varying distributions, once the model is
 520 calibrated in homogeneous conditions, which are more appropriate for the experimental

521 measurement of bacterial parameters. Besides, using a dispersion coefficient value different
 522 from the calibrated one weakened the predictions of the mineralization dynamics but not
 523 the predictions of the mineralization after 24 days, which remained satisfying regardless of
 524 the dispersion coefficient. More precisely, the prediction of the final mineralization became
 525 mostly independent of the dispersion coefficient, as shown for the calibrated model (Fig. 8).
 526 This is because, in the Contois model at low substrate concentrations, the number of active
 527 bacteria in a soil volume is exactly counterbalanced by the regulation of their uptake
 528 efficiency by population density (Eq. (8)), resulting in limited effects of bacterial spreading
 529 on overall mineralization (Fig. 8, constant part of the curves).



530
 531 **Fig. 8.** Influence of the dispersion coefficient on mineralization at day 24 for the
 532 Contois-based models calibrated on the sole hydrostatic experiments (thick red line) and on
 533 both hydrostatic and percolation experiments (thick blue line). For representation and
 534 legend, see Fig. 4.

535 4. Discussion

536 **4.1. Relevance of density control for 2,4-D degradation and soil carbon cycling**

537 4.1.1 *Density control of soil oligotroph bacteria*

538 Bulk soil and highly-diluted environments are usually found to be dominated by bacteria with
539 high maximum uptake efficiency, also called oligotrophs (Fierer et al., 2007; Nunan et al.,
540 2020). Their high maximum uptake efficiency differentiates their life-history strategies and
541 conditions their ability to thrive in resource poor environments (Button, 1993), also
542 assimilated to K-strategy (Tecon and Or, 2017), by opposition to copiotrophic bacteria
543 adapted to rich environments (r-strategy). The maximum uptake efficiency values of the 1%
544 best-fitting parameter sets were of the order of 10^3 - 10^4 l·g⁻¹·d⁻¹ (volume of water per mass
545 of bacteria per unit of time), within the range proposed by Button (1991) to define
546 oligotrophs. Similar or higher maximum uptake efficiency values of the order of
547 10^4 - 10^5 l·g⁻¹·d⁻¹ have been reported for soil oligotrophs (Ohta and Taniguchi, 1988; Zelenev
548 et al., 2005). Values up to $1.64 \cdot 10^5$ have been reported by Tuxen et al. (2002) for 2,4-D
549 degraders in an aerobic aquifer and even greater values might also be possible (see section
550 S5). The high maximum uptake efficiencies predicted in section 3.1 for the best-fitting
551 parameterizations are therefore a plausible bacterial trait among 2,4-D degraders as well as
552 bulk soil bacteria in general. It suggests that density control might be relevant for a
553 component of soil bacteria, which would benefit from dispersion as suggested by Fig. 6. The
554 calibrated model has shown in section 3.2.2 that the values of densities from which
555 competition became critical were around $3.5 \cdot 10^{-3}$ g·l⁻¹, corresponding to $7.5 \cdot 10^{-7}$ g·g (mass
556 of bacteria per mass of dry soil), ranging in the low end of usual total soil bacterial densities

557 (Raynaud and Nunan, 2014; Kuzyakov and Blagodatskaya, 2015). This suggests that
558 competition might play a significant role even under the low bacterial densities observed in
559 bulk soils, at least in similar substrate conditions. Reciprocally, the model suggests that
560 competition for substrate between copiotrophic bacteria only appears at much larger
561 population densities, such as those found in soil biofilms (Holden et al., 1997, Or et al., 2007).
562 Interestingly, copiotrophic bacteria have been reported to cohabit with oligotrophic bacteria
563 even in diluted environments (Gözdereliler et al., 2013). Results from the screening suggest
564 that, for densities of copiotrophs as low as for oligotrophs, their impact on overall
565 decomposition in dilution-dominated environments would be much lower due to their
566 poorly adapted uptake efficiency (Fig. 4A). Conversely, this striking density regulation might
567 be one of the main limitations of the overall population densities in soils. Note that this
568 density regulation occurs within a single population with homogeneous biological constants.
569 Spatial heterogeneities and low substrate concentrations, common in bulk soil, may indeed
570 shift competition from the inter-population level to the intra-population level (Pfeiffer et al.,
571 2001; Roller and Schmidt, 2015).

572 *4.1.2 A new perspective on Regulatory Gate hypothesis*

573 Density regulation might partially contribute to explain the common paradox of the apparent
574 uncoupling between the overall mineralization of a soil volume and the size of its microbial
575 population (Kemmitt et al., 2008). The rate of soil carbon mineralization remains the same
576 even if 90% of the microbial decomposers are killed. This observation is commonly explained
577 by the Regulatory Gate hypothesis, where mineralization is assumed to be controlled by an
578 abiotic process, such as desorption or diffusion, that limits the availability of the substrate,
579 resulting in mineralization rates that are independent of the degrader abundance. We

580 propose that the density regulation of decomposition in oligotrophic environments may
581 contribute to this phenomenon, through competition for substrate or other biological
582 interactions. In the case of competition-related density regulation, it reduces the
583 dependence of the overall carbon mineralization on degrader abundance, as any increase of
584 population density counterbalances the effect of the increased population size. Note that
585 the involved abiotic process, namely the substrate diffusion backward to bacteria (see
586 section 3.2), is well limiting but only in situations of high bacterial competition.

587 ***4.2. Relevance of the ratio-dependent Contois model in soils***

588 As argued in section 3.3, ratio-dependence might facilitate decomposition modeling in the
589 soil conditions typical of the experiments analyzed here. The Contois model's
590 $(1/y) \cdot \mu_{max} / (\kappa_C \cdot B)$ calibrated in homogeneous conditions might be used in heterogeneous
591 conditions more reliably than the Monod model's $(1/y) \cdot \mu_{max} / \kappa_M$, at least for soil systems in
592 which the competition for the substrate plays a substantial role within the degrader
593 population. The similarity between κ_M and $\kappa_C B$ suggests the need to consider population
594 density when measuring the apparent maximum uptake efficiency of soil bacteria to avoid
595 underestimating it by unintentionally including density regulation. Moreover, the better
596 predictions obtained with the Contois model in the soil conditions represented by the
597 experiments suggest that the Contois ratio-dependence includes not only the effect of
598 competition for substrate at the scale of measurement, but it can also reasonably reflect
599 other density processes such as the spatial variability of bacterial distributions at finer scales
600 related to their high degree of local aggregation in microcolonies (Raynaud and Nunan,
601 2014). Moreover, ratio-dependence may also include the cumulative effects of ecological

602 interactions other than competition (Sibly and Hone, 2002). Note that the methodological
603 approach used in this study for both Monod and Contois models is based on an effective
604 representation of concentrations and parameters at the mm- to cm-scale of measurements.
605 These effective concentrations and parameters conceptually integrate the smaller-scale
606 processes highlighted by other studies (Ebrahimi and Or, 2014; Portell et al., 2018; Tecon et
607 al., 2018). Such microscale processes should be addressed for further generalization beyond
608 the conditions of the soil experiments analyzed here. Despite its advantages, Contois models
609 have also a drawback with the fact that the modeled uptake efficiency of bacteria
610 approaches infinity for low densities, which does not correspond to any physical nor
611 biochemical process (Gleeson, 1994; Abrams, 2015). However, this side effect mostly affects
612 a negligible fraction of the bacteria and the substrate, as it was the case in the soil conditions
613 represented by the experiments.

614 Further work is required to confront the relevance of the Contois model to other soil
615 systems. To the best of our knowledge, ratio-dependent growth models such as the Contois
616 model have not yet been considered for the modeling of microbial degradation in soils.
617 However, the Contois growth equation is generally accepted to be more appropriate than
618 the Monod equation for modeling immobilized, heterogeneously distributed or mixed
619 microbial cultures (Arditi and Saiah, 1992; Harmand and Godon, 2007), all of which are
620 characteristics of soils. The regulation of individual activity by population density has
621 frequently been justified as a “crowding effect” associated with high population densities
622 leading to competition for substrate (Lobry and Harmand, 2006; Harmand and Godon, 2007;
623 Krichen et al., 2018). However, little is known about possible density regulation when
624 apparent microbial densities are low, as is observed in bulk soil (Raynaud and Nunan, 2014;

625 Kuzyakov and Blagodatskaya, 2015), although some studies have mentioned
626 ratio-dependence in highly-diluted environments such as aquifers (Hansen et al., 2017). As
627 discussed in section 4.1.1, the high maximum uptake efficiencies commonly observed for soil
628 bacteria adapted to oligotrophic environments are relevant to draw attention on the
629 potential significance of density control at low densities in oligotrophic soils, and thus
630 ratio-dependent models, among which the Contois model is a consistent choice.

631 ***4.3. Hypothetical relationship between bacterial traits and their spatial*** 632 ***strategies***

633 Density regulation might be at the origin of a relationship between bacterial oligotrophy,
634 their location in soil and their mobility strategy. Soil copiotroph bacteria have a maximum
635 uptake efficiency mostly between $100 \text{ l}\cdot\text{g}^{-1}\cdot\text{d}^{-1}$ (Button, 1991) and $800 \text{ l}\cdot\text{g}^{-1}\cdot\text{d}^{-1}$ (Daugherty
636 and Karel, 1994; Zelenev et al., 2005). For copiotrophs with maximum uptake efficiency
637 values below $288 \text{ l}\cdot\text{g}^{-1}\cdot\text{d}^{-1}$, bacterial dispersion was largely detrimental to their activity (Fig. 4
638 blue line, Fig. 6), in agreement with the results of Pagel et al. (2020), suggesting that
639 copiotrophs have more aggregated distributions than oligotrophs. The negligible
640 mineralization even without dispersion (Fig. 3-A4) also highlights the fact that copiotrophs
641 are particularly inefficient at degrading substrates that diffuse in the environment, as also
642 evidenced by Babey et al. (2017). To maintain significant activity, soil copiotrophs are likely
643 to remain immobile in the close surroundings of the substrate source or any immobile
644 substrate, likely attached to surfaces or embedded in EPS matrices. If not, they would be
645 dispersed towards more diluted area where their low maximum uptake efficiency would
646 result in negligible uptake. On the contrary, to survive and develop, soil oligotrophs should

647 be able to easily disperse and escape high competition areas. Given that soil is a poor and
648 heterogeneous environment, this dispersion would be essentially passive (Nunan et al.,
649 2020), through advective processes for example. We therefore suggest the existence of a
650 theoretical relationship between proximity to substrate sources (respectively remoteness),
651 copiotrophy (respectively oligotrophy) and attachment (respectively mobility).

652 **5. Conclusions**

653 Heterogeneous distributions of degraders and substrate in soils strongly control soil organic
654 matter degradation through their interactions with the bacterial activity. Taking 2,4-D as a
655 model organic solute substrate for soil bacteria, we investigated the coupled effects of
656 bacteria and substrate distributions on one side and bacterial traits on the other side on
657 substrate degradation. The analysis of published experiments with contrasted spreading
658 conditions of both bacteria and substrate reveals that, in addition to the distance of bacteria
659 from high substrate concentrations, mineralization is also surprisingly limited by the
660 bacterial density even under the low bacterial densities commonly observed in bulk soils.
661 Moreover, the impact of bacterial dispersion on solute substrate degradation can shift from
662 negative to positive depending on the bacterial maximum uptake efficiency. The activity of
663 soil oligotrophs may be mostly regulated by bacterial density rather than by substrate
664 dilution, echoing the population size paradox regularly observed. It follows that the
665 ratio-dependent Contois model might be more relevant to model bulk soil mineralization in
666 the heterogeneous conditions investigated than the substrate-dependent Monod model. To
667 predict the impact of spatial distributions on degradation in oligotrophic soil, and more
668 particularly the impact of bacterial dispersion, we suggest that bacterial densities might be

669 a more useful measurement than the volumes of soil devoid or occupied with bacteria. With
670 respect to the current lack of direct microscale data on microbial processes and distributions,
671 we propose some key perspectives on the bacterial kinetics and distributions.

672 **Acknowledgements**

673 This work was supported by the Agence Nationale de la Recherche through the project
674 “Soil μ -3D” [grant number ANR-15-CE01-0006] and was also partially supported by the SLAC
675 Floodplain Hydro-Biogeochemistry Science Focus Area (SFA), which is funded by the U.S.
676 Department of Energy (DOE) office of Biological and Environmental Research (BER), Climate
677 and Environmental Sciences Division, under DOE contract No. DE- AC02-76SF00515 to SLAC.
678 The authors thank Jérôme Harmand, Théodore Bouchez, Xavier Raynaud, Tanguy Le Borgne,
679 Claire Chenu and Holger Pagel for insightful discussions. The authors would also like to thank
680 the two anonymous referees and the editor for their constructive and valuable comments.

681 **Appendix A. Supplementary Data**

682 **References**

- 683 Abrams, P.A., 2015. Why ratio dependence is (still) a bad model of predation: Ratio-
684 dependent predation. *Biological Reviews* 90, 794–814.
685 <https://doi.org/10.1111/brv.12134>
- 686 Arditi, R., Saiah, H., 1992. Empirical evidence of the role of heterogeneity in ratio-
687 dependent consumption. *Ecology* 73, 1544–1551. <https://doi.org/10.2307/1940007>

688 Babey, T., Vieublé Gonod, L., Rapaport, A., Pinheiro, M., Garnier, P., de Dreuzy, J.-R., 2017.
689 Spatiotemporal simulations of 2,4-D pesticide degradation by microorganisms in 3D
690 soil-core experiments. *Ecological Modelling* 344, 48–61.
691 <https://doi.org/10.1016/j.ecolmodel.2016.11.006>

692 Bælum, J., Henriksen, T., Hansen, H.C.B., Jacobsen, C.S., 2006. Degradation of 4-chloro-2-
693 methylphenoxyacetic acid in top- and subsoil is quantitatively linked to the class III
694 *tfdA* gene. *Applied and Environmental Microbiology* 72, 1476–1486.
695 <https://doi.org/10.1128/AEM.72.2.1476-1486.2006>

696 Bælum, J., Nicolaisen, M.H., Holben, W.E., Strobel, B.W., Sørensen, J., Jacobsen, C.S., 2008.
697 Direct analysis of *tfdA* gene expression by indigenous bacteria in phenoxy acid
698 amended agricultural soil. *The ISME Journal* 2, 677–687.
699 <https://doi.org/10.1038/ismej.2008.21>

700 Boivin, A., Amellal, S., Schiavon, M., van Genuchten, M.Th., 2005. 2,4-
701 dichlorophenoxyacetic acid (2,4-D) sorption and degradation dynamics in three
702 agricultural soils. *Environmental Pollution* 138, 92–99.
703 <https://doi.org/10.1016/j.envpol.2005.02.016>

704 Breitenbeck, G.A., Yang, H., Dunigan, E.P., 1988. Water-facilitated dispersal of inoculant
705 *Bradyrhizobium japonicum* in soils. *Biology and Fertility of Soils* 7, 58–62.
706 <https://doi.org/10.1007/BF00260733>

707 Bünemann, E.K., Bongiorno, G., Bai, Z., Creamer, R.E., De Deyn, G., de Goede, R., Fleskens,
708 L., Geissen, V., Kuyper, T.W., Mäder, P., Pulleman, M., Sukkel, W., van Groenigen,
709 J.W., Brussaard, L., 2018. Soil quality – A critical review. *Soil Biology and*
710 *Biochemistry* 120, 105–125. <https://doi.org/10.1016/j.soilbio.2018.01.030>

711 Button, D.K., 1978. On the theory of control of microbial growth kinetics by limiting
712 nutrient concentrations. *Deep Sea Research* 25, 1163–1177.
713 [https://doi.org/10.1016/0146-6291\(78\)90011-5](https://doi.org/10.1016/0146-6291(78)90011-5)

714 Button, D.K., 1983. Differences between the kinetics of nutrient uptake by micro-
715 organisms, growth and enzyme kinetics. *Trends in Biochemical Sciences* 8, 121–124.
716 [https://doi.org/10.1016/0968-0004\(83\)90232-3](https://doi.org/10.1016/0968-0004(83)90232-3)

717 Button, D.K., 1991. Biochemical basis for whole-cell uptake kinetics: specific affinity,
718 oligotrophic capacity, and the meaning of the michaelis constant. *Applied and*
719 *Environmental Microbiology* 57, 2033–2038.

720 Button, D.K., 1993. Nutrient-limited microbial growth kinetics: overview and recent
721 advances. *Antonie van Leeuwenhoek* 63, 225–235.
722 <https://doi.org/10.1007/BF00871220>

723 Carrayrou, J., Mosé, R., Behra, P., 2004. Operator-splitting procedures for reactive
724 transport and comparison of mass balance errors. *Journal of Contaminant*
725 *Hydrology* 68, 239–268. doi:10.1016/S0169-7722(03)00141-4

726 Cheyns, K., Mertens, J., Diels, J., Smolders, E., Springael, D., 2010. Monod kinetics rather
727 than a first-order degradation model explains atrazine fate in soil mini-columns:
728 Implications for pesticide fate modelling. *Environmental Pollution* 158, 1405–1411.
729 <https://doi.org/10.1016/j.envpol.2009.12.041>

730 Contois, D.E., 1959. Kinetics of bacterial growth: relationship between population density
731 and specific growth rate of continuous cultures. *Journal of General Microbiology* 21,
732 40–50. <https://doi.org/10.1099/00221287-21-1-40>

733 Daugherty, D.D., Karel, S.F., 1994. Degradation of 2,4-dichlorophenoxyacetic acid by
734 *Pseudomonas cepacia* DBOL(pRO101) in a dual-substrate chemostat. *Applied and*
735 *Environmental Microbiology* 60, 3261–3267.

736 Dechesne, A., Owsianiak, M., Bazire, A., Grundmann, G.L., Binning, P.J., Smets, B.F., 2010.
737 Biodegradation in a partially saturated sand matrix: compounding effects of water
738 content, bacterial spatial distribution, and motility. *Environmental Science &*
739 *Technology* 44, 2386–2392. <https://doi.org/10.1021/es902760y>

740 Dechesne, A., Badawi, N., Aamand, J., Smets, B.F., 2014. Fine scale spatial variability of
741 microbial pesticide degradation in soil: scales, controlling factors, and implications.
742 *Frontiers in Microbiology* 5, 667. <https://doi.org/10.3389/fmicb.2014.00667>

743 Desmond-Le Quéméner, E., Bouchez, T., 2014. A thermodynamic theory of microbial
744 growth. *The ISME Journal* 8, 1747–1751. doi:10.1038/ismej.2014.7

745 Don, R.H., Weightman, A.J., 1985. Transposon mutagenesis and cloning analysis of the
746 pathways for degradation of 2,4-dichlorophenoxyacetic acid and 3-chlorobenzoate
747 in *Alcaligenes eutrophus* JMP134(pJP4). *Journal of Bacteriology* 161, 85–90.

748 Ebrahimi, A.N., Or, D., 2014. Microbial dispersal in unsaturated porous media:
749 Characteristics of motile bacterial cell motions in unsaturated angular pore
750 networks. *Water Resources Research* 50, 7406–7429. doi:10.1002/2014WR015897

751 Fierer, N., Bradford, M.A., Jackson, R.B., 2007. Toward an ecological classification of soil
752 bacteria. *Ecology* 88, 1354–1364. <https://doi.org/10.1890/05-1839>

753 Gleeson, S.K., 1994. Density dependence is better than ratio dependence. *Ecology* 75,
754 1834–1835. <https://doi.org/10.2307/1939642>

755 Gözdereliler, E., Boon, N., Aamand, J., De Roy, K., Granitsiotis, M.S., Albrechtsen, H.J.,
756 Sørensen, S.R., 2013. Comparing metabolic functionalities, community structures
757 and dynamics of herbicide-degrading communities with different substrate
758 concentrations. *Applied and Environmental Microbiology* 79 (1), 367–375.
759 <https://doi.org/10.1128/AEM.02536-12>

760 Hansen, S.K., Pandey, S., Karra, S., Vesselinov, V.V., 2017. CHROTRAN: A mathematical and
761 computational model for in situ heavy metal remediation in heterogeneous
762 aquifers. *ArXiv:1703.01381 [q-Bio]*.

763 Harmand, J., Godon, J.J., 2007. Density-dependent kinetics models for a simple description
764 of complex phenomena in macroscopic mass-balance modeling of bioreactors.
765 *Ecological Modelling* 200, 393–402.
766 <https://doi.org/10.1016/j.ecolmodel.2006.08.012>

767 Healey, F.P., 1980. Slope of the Monod equation as an indicator of advantage in nutrient
768 competition. *Microbial Ecology* 5, 281–286. <http://www.jstor.org/stable/4250586>

769 Holden, P.A., Firestone, M.K., 1997. Soil microorganisms in soil cleanup: How can we
770 improve our understanding? *Journal of Environment Quality* 26, 32–40.
771 <https://doi.org/10.2134/jeq1997.00472425002600010006x>

772 Holden, P.A., Hunt, J.R., Firestone, M.K., 1997. Toluene diffusion and reaction in
773 unsaturated *Pseudomonas putida* biofilms. *BIOTECHNOLOGY AND*
774 *BIOENGINEERING* 56, 15.

775 Iserles, A., 2009. *A first course in the numerical analysis of differential equations*,
776 Cambridge University Press. ed.

777 Kemmitt, S.J., Lanyon, C.V., Waite, I.S., Wen, Q., Addiscott, T.M., Bird, N.R.A., O'Donnell,
778 A.G., Brookes, P.C., 2008. Mineralization of native soil organic matter is not
779 regulated by the size, activity or composition of the soil microbial biomass—a new
780 perspective. *Soil Biology and Biochemistry* 40, 61–73.
781 <https://doi.org/10.1016/j.soilbio.2007.06.021>

782 König, S., Vogel, H.-J., Harms, H., Worrlich, A., 2020. Physical, chemical and biological effects
783 on soil bacterial dynamics in microscale models. *Frontiers in Ecology and Evolution*
784 8, 53. <https://doi.org/10.3389/fevo.2020.00053>

785 Krichen, E., Harmand, J., Torrijos, M., Godon, J.J., Bernet, N., Rapaport, A., 2018. High
786 biomass density promotes density-dependent microbial growth rate. *Biochemical*
787 *Engineering Journal* 130, 66–75. <https://doi.org/10.1016/j.bej.2017.11.017>

788 Kuzyakov, Y., Blagodatskaya, E., 2015. Microbial hotspots and hot moments in soil: Concept
789 & review. *Soil Biology and Biochemistry* 83, 184–199.
790 <https://doi.org/10.1016/j.soilbio.2015.01.025>

791 Lagneau, V., van der Lee, J., 2010. Operator-splitting-based reactive transport models in
792 strong feedback of porosity change: The contribution of analytical solutions for
793 accuracy validation and estimator improvement. *Journal of Contaminant Hydrology*
794 112, 118–129. doi:10.1016/j.jconhyd.2009.11.005

795 Lobry, C., Harmand, J., 2006. A new hypothesis to explain the coexistence of n species in
796 the presence of a single resource. *Comptes Rendus Biologies* 329, 40–46.
797 <https://doi.org/10.1016/j.crv.2005.10.004>

798 Lobry, J.R., Flandrois, J.P., Carret, G., Pave, A., 1992. Monod's bacterial growth model
799 revisited. *Bulletin of Mathematical Biology* 54, 117–122.
800 <https://doi.org/10.1007/BF02458623>

801 Madsen, E.L., Alexander, M., 1982. Transport of Rhizobium and Pseudomonas through Soil.
802 *Soil Science Society of America Journal* 46, 557–560.
803 <https://doi.org/10.2136/sssaj1982.03615995004600030023x>

804 Monod, J., 1949. The growth of bacterial cultures. *Annual Review of Microbiology* 3, 371–
805 394. <https://doi.org/10.1146/annurev.mi.03.100149.002103>

806 Nunan, N., Young, I.M., Crawford, J.W., Ritz, K., 2007. Bacterial interactions at the
807 microscale - Linking habitat to function in soil, in: Franklin, R., Mills, A. (Eds.), *The*
808 *Spatial Distribution of Microbes in the Environment*. Springer, Dordrecht, pp. 61–85.

809 Nunan, N., Schmidt, H., Raynaud, X., 2020. The ecology of heterogeneity: soil bacterial
810 communities and C dynamics. *Philosophical Transactions of the Royal Society B:*
811 *Biological Sciences* 375, 20190249. <https://doi.org/10.1098/rstb.2019.0249>

812 Ohta, H., Taniguchi, S., 1988. Growth characteristics of the soil oligotrophic bacterium:
813 *Agromonas oligotrophica* JCM 1494 on diluted nutrient broth. *The Journal of*
814 *General and Applied Microbiology* 34, 349–353.
815 <https://doi.org/10.2323/jgam.34.349>

816 Or, D., Smets, B.F., Wraith, J.M., Dechesne, A., Friedman, S.P., 2007. Physical constraints
817 affecting bacterial habitats and activity in unsaturated porous media – a review.
818 *Advances in Water Resources* 30, 1505–1527. doi:10.1016/j.advwatres.2006.05.025

819 Pagel, H., Kriesche, B., Uksa, M., Poll, C., Kandeler, E., Schmidt, V., Streck, T., 2020. Spatial
820 control of carbon dynamics in soil by microbial decomposer communities. *Frontiers*
821 in *Environmental Science* 8, 2. <https://doi.org/10.3389/fenvs.2020.00002>

822 Pallud, C., Dechesne, A., Gaudet, J.P., Debouzie, D., Grundmann, G.L., 2004. Modification of
823 spatial distribution of 2,4-dichlorophenoxyacetic acid degrader microhabitats during
824 growth in soil columns. *Applied and Environmental Microbiology* 70, 2709–2716.
825 <https://doi.org/10.1128/AEM.70.5.2709-2716.2004>

826 Patarinska, T., Dochain, D., Agathos, S.N., Ganovski, L., 2000. Modelling of continuous
827 microbial cultivation taking into account the memory effects. *Bioprocess*
828 *Engineering* 22, 517–527. <https://doi.org/10.1007/s004499900095>

829 Pfeiffer, T., Schuster, S., Bonhoeffer, S., 2001. Cooperation and Competition in the
830 Evolution of ATP-Producing Pathways 292, 5.

831 Pieper, D.H., Reineke, W., Engesser, K.-H., Knackmuss, H.-J., 1988. Metabolism of 2,4-
832 dichlorophenoxyacetic acid, 4-chloro-2-methylphenoxyacetic acid and 2-
833 methylphenoxyacetic acid by *Alcaligenes eutrophus* JMP 134. *Archives of*
834 *Microbiology* 150, 95–102. <https://doi.org/10.1007/BF00409724>

835 Pinheiro, M., Garnier, P., Beguet, J., Martin Laurent, F., Vieublé Gonod, L., 2015. The
836 millimetre-scale distribution of 2,4-D and its degraders drives the fate of 2,4-D at
837 the soil core scale. *Soil Biology and Biochemistry* 88, 90–100.
838 <https://doi.org/10.1016/j.soilbio.2015.05.008>

839 Pinheiro, M., Pagel, H., Poll, C., Ditterich, F., Garnier, P., Streck, T., Kandeler, E., Vieublé
840 Gonod, L., 2018. Water flow drives small scale biogeography of pesticides and
841 bacterial pesticide degraders - A microcosm study using 2,4-D as a model

842 compound. *Soil Biology and Biochemistry* 127, 137–147.
843 <https://doi.org/10.1016/j.soilbio.2018.09.024>

844 Poll, C., Ingwersen, J., Stemmer, M., Gerzabek, M.H., Kandeler, E., 2006. Mechanisms of
845 solute transport affect small-scale abundance and function of soil microorganisms
846 in the detritosphere. *European Journal of Soil Science* 57, 583–595.
847 <https://doi.org/10.1111/j.1365-2389.2006.00835.x>

848 Portell, X., Pot, V., Garnier, P., Otten, W., Baveye, P.C., 2018. Microscale Heterogeneity of
849 the Spatial Distribution of Organic Matter Can Promote Bacterial Biodiversity in
850 Soils: Insights From Computer Simulations. *Frontiers in Microbiology* 9, 1583.
851 [doi:10.3389/fmicb.2018.01583](https://doi.org/10.3389/fmicb.2018.01583)

852 Raynaud, X., Nunan, N., 2014. Spatial Ecology of Bacteria at the Microscale in Soil. *PLoS*
853 *ONE* 9, e87217. <https://doi.org/10.1371/journal.pone.0087217>

854 Roller, B.R., Schmidt, T.M., 2015. The physiology and ecological implications of efficient
855 growth. *The ISME Journal* 9, 1481–1487. <https://doi.org/10.1038/ismej.2014.235>

856 Shampine, L.F., Reichelt, M.W., 1997. The MATLAB ODE Suite. *SIAM Journal on Scientific*
857 *Computing* 18, 1–22. <https://doi.org/10.1137/S1064827594276424>

858 Sibly, R.M., Hone, J., 2002. Population growth rate and its determinants: an overview.
859 *Philosophical Transactions of the Royal Society of London. Series B: Biological*
860 *Sciences* 357, 1153–1170. <https://doi.org/10.1098/rstb.2002.1117>

861 Sinton, G.L., Fan, L.T., Erickson, L.E., Lee, S.M., 1986. Biodegradation of 2,4-D and related
862 xenobiotic compounds. *Enzyme and Microbial Technology* 8, 395–403.
863 [https://doi.org/10.1016/0141-0229\(86\)90145-6](https://doi.org/10.1016/0141-0229(86)90145-6)

864 Stana, R.L., 2020. Diffusive transport: theory and application (Doctor of Philosophy thesis).
865 University of Leeds, UK.

866 Tecon, R., Or, D., 2017. Biophysical processes supporting the diversity of microbial life in
867 soil. *FEMS Microbiology Reviews* 41, 599–623.
868 <https://doi.org/10.1093/femsre/fux039>

869 Tecon, R., Ebrahimi, A., Kleyer, H., Erev Levi, S., Or, D., 2018. Cell-to-cell bacterial
870 interactions promoted by drier conditions on soil surfaces. *Proceedings of the*
871 *National Academy of Sciences* 115, 9791–9796. doi:10.1073/pnas.1808274115

872 Tuxen, N., de Liphay, J.R., Albrechtsen, H.-J., Aamand, J., Bjerg, P.L., 2002. Effect of
873 exposure history on microbial herbicide degradation in an aerobic aquifer affected
874 by a point source. *Environmental Science & Technology* 36, 2205–2212.
875 <https://doi.org/10.1021/es0113549>

876 Ugalde-Salas, P., Desmond-Le Quéméner, E., Harmand, J., Rapaport, A., Bouchez, T., 2020.
877 Insights from Microbial Transition State Theory on Monod's Affinity Constant.
878 *Scientific Reports* 10, 5323. doi:10.1038/s41598-020-62213-6

879 Vieublé Gonod, L., Chenu, C., Soulas, G., 2003. Spatial variability of 2,4-
880 dichlorophenoxyacetic acid (2,4-D) mineralisation potential at a millimetre scale in
881 soil. *Soil Biology and Biochemistry* 35, 373–382. [https://doi.org/10.1016/S0038-](https://doi.org/10.1016/S0038-0717(02)00287-0)
882 [0717\(02\)00287-0](https://doi.org/10.1016/S0038-0717(02)00287-0)

883 Young, I.M., Crawford, J.W., Nunan, N., Otten, W., Spiers, A., 2008. Chapter 4 Microbial
884 distribution in soils, in: *Advances in Agronomy*. Elsevier, pp. 81–121.
885 [https://doi.org/10.1016/S0065-2113\(08\)00604-4](https://doi.org/10.1016/S0065-2113(08)00604-4)

886 Zelenev, V.V., van Bruggen, A.H.C., Semenov, A.M., 2005. Modeling wave-like dynamics of
887 oligotrophic and copiotrophic bacteria along wheat roots in response to nutrient
888 input from a growing root tip. *Ecological Modelling* 188, 404–417.
889 <https://doi.org/10.1016/j.ecolmodel.2005.01.046>